Iterative Low-rank and rotating sparsity promotion for circumstellar disks imaging

Benoît Pairet and Laurent Jacques
ISPGroup, ICTEAM
UCLouvain, Belgium

Faustine Cantalloube
Max Planck Institute for Astronomy
Heidelberg, Germany

***Abstract*—Recent astronomical observations open the possibility to directly image circumstellar disks, a key feature for our understanding of extra-solar systems. However, the faint intensity of these celestial signals compared to the brightness of their hosting star make their accurate characterization a challenging processing task. While there exist several post processing techniques adapted to the extraction of (point shaped) exoplanets, this work proposes a novel iterative method for extracting the elongated structure of circumstellar signals from direct imaging datasets. This method leverages low-complexity models of both the corrupting stellar light and the disks. Our approach is assessed through numerical experiments.**

Context: Imaging stellar systems requires devices enabling both high contrast and high resolution observations to be able to distinguish the faint objects lying near the much brighter hosting star. Ground based telescopes offer the highest resolution but suffer from atmospheric turbulence. Even with state-of-the-art hardware (adaptive optics to correct the wavefront and a coronagraph to hide most of the starlight), residual quasi-statics aberrations, forming *speckles* in the image, prevent detection of faint objects (see Fig. 1). Specific observation methods are thus used to increase data diversity and disentangle the on-sky signals from the speckles.

Angular differential imaging (ADI) is a popular observation strategy [1] where multiple snapshots of the star are taken through a night of observation in a way such that the speckles remain quasi-static while on-sky signals follow a deterministic circular trajectory, determined by tabulated parallactic angles. Dedicated processing is then required to process ADI datasets. Among them, Principal Components Analysis (PCA) is a popular method to reduce the observation to a more interpretable signal [2], [3]. The processing pipeline goes as follows: *(i)* the $T \times (n \times n)$ (with n^2 the number of pixels of each image and T the number of frames) spatiotemporal data cube is reshaped into a $\mathbb{R}^{T\times n^2}$ matrix $\boldsymbol{Y}$, *(ii)* we compute its rank-r approximation by thresholding its singular values decomposition (SVD) to its r strongest singular values, we denote this operation by $\boldsymbol{L} = \mathcal{H}_r^{\rm SVD}(\boldsymbol{Y})$, *(iii)* $\boldsymbol{L}$ is then subtracted from the data to form $\boldsymbol{S} = \boldsymbol{Y} - \boldsymbol{L}$ containing the on-sky signals, and *(iv)* the frames of $\boldsymbol{S}$ are aligned (by rotation and interpolation) to the on-sky coordinates and temporally averaged to form the processed frame. Object detection is then usually performed afterwards [4], [5].

Limitations with disks: The morphology of the disks is known to be severely impacted by the reduction procedure, hindering our capability to study the structure of the disks from ADI datasets. Results of PCA on the ellipsoidal disk surrounding HR 4796A [6] is displayed on Fig. 2, where we can see unphysical negative artifacts. There have only been few attempts to tackle the post-processing induced deformation on disk from ADI datasets. We mention [7], where the authors estimate the PCA-induced deformation by injecting disks that they estimate by forward-modeling. Others have used non-negative matrix factorization but in a slightly different context [8].

Our approach: We restart from a reshaped ADI sequence $\boldsymbol{Y} \in \mathbb{R}^{T\times n^2}$. Assuming $\boldsymbol{Y}$ contains a disk, a realistic mixing model for the different observed signals reads

$$\boldsymbol{Y} = \boldsymbol{Y}_{\rm star} + \boldsymbol{Y}_{\rm disk} + \boldsymbol{N}, \tag{1}$$

where $\boldsymbol{Y}_{\rm star}$ is the starlight, $\boldsymbol{Y}_{\rm disk}$ is the disc, and $\boldsymbol{N}$ is some undefined low intensity noise. In (1), $\boldsymbol{Y}_{\rm star}$ is further modeled as the sum of a temporally static term $\boldsymbol{Y}_{\rm static}$ and a non-static term $\boldsymbol{N}_s$. Hence the forward model becomes:

$$\boldsymbol{Y} = \boldsymbol{Y}_{\rm static} + \boldsymbol{N}_s + \boldsymbol{Y}_{\rm disk} + \boldsymbol{N}, \tag{2}$$

Each component of the model (2) can be characterized by a specific prior or behavior: $\boldsymbol{Y}_{\rm static}$ can be associated to a low-rank structure, $\boldsymbol{N}_s + \boldsymbol{N}$ is treated as noise, and, as the intensity of $\boldsymbol{Y}_{\rm disk}$ on the on-sky coordinates is constant through time, it can be modeled as the rotating image of the disk. Additionally, as we expect the some spatial structure in the disk, we assume it to be sparsely represented in a wavelet basis $\boldsymbol{\Psi}$. From these considerations, we pose the estimation of the disk image $\hat{\boldsymbol{x}}$ as this minimization program

$$(\hat{\boldsymbol{L}}, \hat{\boldsymbol{x}}) \in \operatorname{argmin}_{\boldsymbol{L},\boldsymbol{x}} \quad {}^1\!/\!_2\|\boldsymbol{Y} - \boldsymbol{L} - R(\boldsymbol{p}\boldsymbol{x}^\top)\|_2^2, \tag{3}$$

$$\text{s.t.} \quad \operatorname{rank}(\boldsymbol{L}) \leqslant k, \qquad \|\boldsymbol{\Psi}^\top \boldsymbol{x}\|_0 \leqslant s, \tag{4}$$

with $\boldsymbol{p}$ some given intensity vector and $R : \mathbb{R}^{T\times n^2} \to \mathbb{R}^{T\times n^2}$ the linear operator that rotates each frame of the volume using the opposite parallactic angles. Note that given $\boldsymbol{x}$, $R(\boldsymbol{p}\boldsymbol{x}^\top)$ stands for the spatiotemporal ADI observation of the disk alone (without any starlight nor noise). As our optimization scheme is NP-hard (from the ℓ_0 constraint), we propose to approximate by a variant of the iterative hard thresholding (IHT) algorithm, *i.e.*, alternating between a gradient descent over the cost in (3) and a projection on its non-convex constraints. First, we write $\boldsymbol{U} = (\boldsymbol{L}^\top, \boldsymbol{x})^\top \in \mathbb{R}^{(T+1)\times n^2}$ and $\mathcal{L} := \mathcal{L}(\boldsymbol{U}, \boldsymbol{Y}) = \frac{1}{2}\|\boldsymbol{Y} - \boldsymbol{S}_{\boldsymbol{L}}(\boldsymbol{U}) - R(\boldsymbol{p}\boldsymbol{S}_{\boldsymbol{x}}(\boldsymbol{U}))\|_2^2$, where $\boldsymbol{S}_{\boldsymbol{L}}$ and $\boldsymbol{S}_{\boldsymbol{x}}$ are selection operators, selecting $\boldsymbol{L}$ and $\boldsymbol{x}^\top$ from $\boldsymbol{U}$, respectively. Second, we compute

$$\nabla_{\boldsymbol{U}}\mathcal{L} = \begin{pmatrix} \nabla_{\boldsymbol{L}}\mathcal{L} \\ \nabla_{\boldsymbol{x}^\top}\mathcal{L} \end{pmatrix} = \begin{pmatrix} \boldsymbol{L} + R(\boldsymbol{p}\boldsymbol{x}^\top) - \boldsymbol{Y} \\ \|\boldsymbol{p}\|_2^2 \boldsymbol{x}^\top + \boldsymbol{p}^\top R^\top(\boldsymbol{L} - \boldsymbol{Y}) \end{pmatrix}. \tag{5}$$

Third, the respect of the constraints (4) is ensured by applying the operator $H_{r,s}(\boldsymbol{U})$ defined as

$$\mathcal{H}_{r,s}(\boldsymbol{U}) = \begin{pmatrix} \mathcal{H}_r^{\rm SVD}(\boldsymbol{S}_{\boldsymbol{L}}(\boldsymbol{U})) \\ \mathcal{H}_s(\boldsymbol{S}_{\boldsymbol{x}}(\boldsymbol{U})\boldsymbol{\Psi})\boldsymbol{\Psi}^\top \end{pmatrix}.$$

Finally, from the initialization $\boldsymbol{U}^0 = \boldsymbol{Y}$, our iterative algorithm reads

$$\boldsymbol{U}^{n+1} = \mathcal{H}_{r,s}(\boldsymbol{U}^n - \mu\nabla_{\boldsymbol{U}}\mathcal{L}(\boldsymbol{U}^n, \boldsymbol{Y})). \tag{6}$$

To quantitatively compare our algorithm to PCA, we created a synthetic dataset. We first constructed a speckle field, modeled by $T \times n \times n$ Laplacian random noise [5] with mean and standard deviation mimicking the speckle of a real dataset. Then this volume is convolved with a temporal correlation window. Second this dataset is constrained to be exactly of rank 10. We then inject a disk (Fig. 4) and apply both PCA (Fig. 5) and IHT (Fig. 6). We can see that our algorithm outperforms PCA.

Finally, in Fig. 3, we have tested our algorithm on the HR 4796A dataset. Compared to the PCA reduction, the detected disk is not corrupted by the unphysical, negative artifacts.

BP and LJ are funded by the Belgian F.R.S.-FNRS. The authors thank Julien Milli and Anne-Lise Maire for kindly providing the SPHERE datasets used in this study.

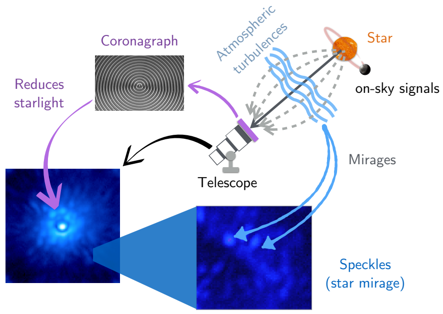

Fig. 1: Schematic view of the underlying physics.

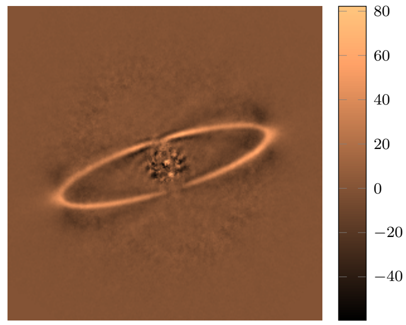

Fig. 2: Post-processed image the disk surrounding HR 4796A obtained with PCA. The PCA frame exhibit the typical unphysical negative artifacts.

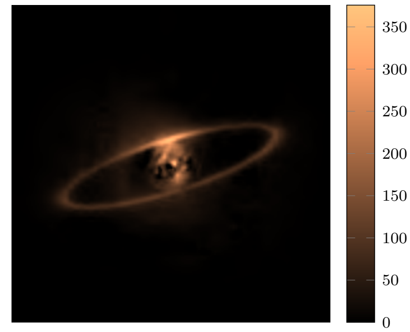

Fig. 3: Post-processed image the disk surrounding HR 4796A obtained with our algorithm. Contrary to PCA, our approach yields a physically plausible image.

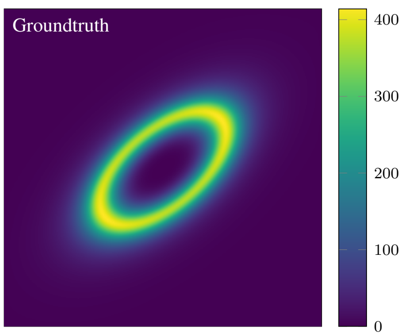

Fig. 4: Groundtruth of the synthetic data.

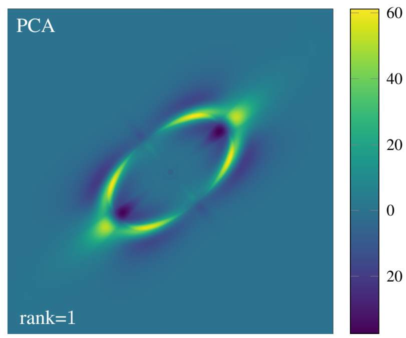

Fig. 5: Results with PCA. The mean squared error is 9596.

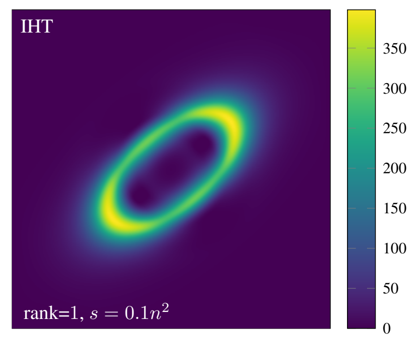

Fig. 6: Result with our algorithm. The mean squared error is 487.

REFERENCES

[1] C. Marois, D. Lafreniere, R. Doyon, B. Macintosh, and D. Nadeau, "Angular differential imaging: A powerful high-contrast imaging technique." *The Astrophysical Journal*, vol. 641, no. 1, p. 556, 2006.

[2] R. Soummer, L. Pueyo, and J. Larkin, "Detection and characterization of exoplanets and disks using projections on karhunen-loève eigenimages," *The Astrophysical Journal Letters*, vol. 755, no. 2, p. L28, 2012.

[3] A. Amara and S. P. Quanz, "Pynpoint: an image processing package for finding exoplanets," *Monthly Notices of the Royal Astronomical Society*, vol. 427, no. 2, pp. 948–955, 2012.

[4] D. Mawet, J. Milli, Z. Wahhaj, D. Pelat, O. Absil, C. Delacroix, A. Boccaletti, M. Kasper, M. Kenworthy, C. Marois, *et al.*, "Fundamental limitations of high contrast imaging set by small sample statistics," *The Astrophysical Journal*, vol. 792, no. 2, p. 97, 2014.

[5] B. Pairet, F. Cantalloube, C. A. Gomez Gonzalez, O. Absil, and L. Jacques, "Stim map: detection map for exoplanets imaging beyond asymptotic gaussian residual speckle noise," *Submitted in Monthly Notices of the Royal Astronomical Society*, 2018.

[6] J. Milli, A. Vigan, D. Mouillet, A.-M. Lagrange, J.-C. Augereau, C. Pinte, D. Mawet, H. M. Schmid, A. Boccaletti, L. Matrà, *et al.*, "Near-infrared scattered light properties of the hr 4796 a dust ring-a measured scattering phase function from 13.6 to 166.6," *Astronomy & Astrophysics*, vol. 599, p. A108, 2017.

[7] J. Milli, D. Mouillet, A.-M. Lagrange, A. Boccaletti, D. Mawet, G. Chauvin, and M. Bonnefoy, "Impact of angular differential imaging on circumstellar disk images," *Astronomy & Astrophysics*, vol. 545, p. A111, 2012.

[8] B. Ren, L. Pueyo, G. B. Zhu, J. Debes, and G. Duchêne, "Non-negative matrix factorization: Robust extraction of extended structures," *The Astrophysical Journal*, vol. 852, no. 2, p. 104, 2018.